Supporting information

Simultaneous production of hydrogen and chlorine through overall brine splitting with a particulate photocatalyst

Takumi Okada,[ab] Masanori Kodera,[a] Yugo Miseki,[a] Hitoshi Kusama,[a] Takahiro Gunji,[b] and Kazuhiro Sayama*[ab]*

[a] Global Zero Emission Research Center (GZR), National Institute of Advanced Industrial Science and Technology (AIST), Tsukuba West, 16-1, Onogawa, Tsukuba, Ibaraki, 305-8569 Japan

[b] Department of Pure and Applied Chemistry, Faculty of Science and Technology, Tokyo University of Science, 2641 Yamazaki, Noda, Chiba 278-8510, Japan

Corresponding Authors

*Kazuhiro Sayama. E-mail address: k.sayama@aist.go.jp

*Masanori Kodera. E-mail address: masanori.kodera@aist.go.jp

Contents

Experimental details

TiO$_2$ (rutile, 99.9%; Kojundo Chemical) was modified with a Pt cocatalyst by *in situ* photodeposition, in which the metal nanoparticles were deposited on the reducing sites of the photocatalyst. Briefly, TiO$_2$ (500 mg) was dispersed in a 10 vol% methanol solution (400 mL) containing an appropriate amount of H$_2$PtCl$_6$•6H$_2$O (98.5+%; FUJIFILM Wako Pure Chemical) using a magnetic stirrer. The resulting mixture was irradiated overnight with 365 nm LED light (CL-1501; Asahi Spectra; see Fig. S9). The obtained powder specimen was filtered, washed with pure water, and then dried at room temperature overnight. X-ray diffractometry (XRD; PANalytical, EMPYREAN) analysis of the TiO$_2$ powder confirmed the existence of the rutile phase as the main phase structure (Fig. S2).

The photocatalytic reactions were performed in an Ar flow system (1 atm, 5 mL min^{-1}; Fig. S3). Briefly, the photocatalyst powder was suspended in a 500 mM NaCl aqueous solution added to a Pyrex side-irradiation cell. The pH of the reactant solution was adjusted using HClO$_4$ (70.0%–72.0%; FUJIFILM Wako Pure Chemical) or NaOH (97.0+%; FUJIFILM Wako Pure Chemical). The aforementioned LED lamp was used as the light source. The amounts of evolved H$_2$ and O$_2$ were determined by gas chromatography (3000A Micro GC device with an MS-5A column, thermal conductivity detector, and Ar carrier; Agilent Technologies). The Cl$_2$ evolved as gas was trapped in a 4 M NaOH solution to form hypochlorite ions (ClO$^-$), whose amount was calculated using the N,N′-bis(2,4-di-sulfobenzyl)tolidine tetrasodium salt method. The total photon flux from LED light was calculated to be 8.5×10^{17} s^{-1}, which was used for calculating the quantum efficiency.

In this study, the e$^-$/h$^+$ ratio was calculated by the following equation:

e$^-$/h$^+$ = 2×(amount of produced H$_2$)/{2×(amount of produced Cl$_2$ detected in the NaOH trap) + 2×(amount of produced HClO and ClO$^-$ in the reaction cell) + 4×(amount of O$_2$)},

where, it is confirmed that the amount of HClO and ClO$^-$ in the reaction cell was negligible.

A TiO$_2$/Ti photoelectrode was prepared by calcining a Ti plate (2 × 3 cm^2) at 973 K for 1 h. As shown in Fig. S13, peaks attributable to rutile and Ti substrate were observed while peaks from anatase or other phases were negligible, which is a similar situation in powder TiO$_2$ used in the experiments. Pt was modified by photodeposition in a manner similar to that of the particulate photocatalyst.

UV-light-driven photoelectrochemical HClO production was studied using a three-electrode system containing TiO$_2$/Ti, Pt wire, and Ag/AgCl as the photoanode, counter electrode, and reference electrode, respectively. The photoanode was immersed in a 500 mM aqueous NaCl solution (30 mL) and illuminated under 365 nm LED light while Ar was bubbled into the anode chamber at 5 mL min^{-1}. External bias *vs.* Ag/AgCl was monitored using a potentiostat (ALS627E, BAS Inc.) while maintaining the anode photocurrent at 0.8 mA. H$_2$, O$_2$, and HClO were similarly quantified.

Computational details

Density functional theory (DFT) calculations were performed using Gaussian 16 software.[1] The ground-state geometry was optimized at the hybrid DFT level using the B3LYP functional, which combines Becke's three-parameter exchange function (B3)[2] with the Lee–Yang–Parr (LYP) correlation function.[3] The Pople-type split-valence basis set 6-311+G(d,p)[4] was used for all the systems.[5] The B3LYP/6-311+G(d,p) level provides appropriate geometries for isolated molecules such as H_2O, O_2, as well as TiO_2.[6,7] Frequency calculations were performed to confirm the optimized structures with no imaginary frequencies, which corresponded to real minima on the entire potential energy surface. Furthermore, they were used to compute zero-point vibrational energies.

Cl_2 formation via two-electron oxidation was considered for two HCl molecules on the metal oxide, as follows:

$$2HCl \rightarrow Cl_2 + 2(H^+ + e^-). \qquad (S1)$$

For comparison, the mechanism of H_2O oxidation on TiO_2—which involves four proton-coupled electron-transfer (PCET) steps with two H_2O molecules, as shown below—was investigated.[8–13]
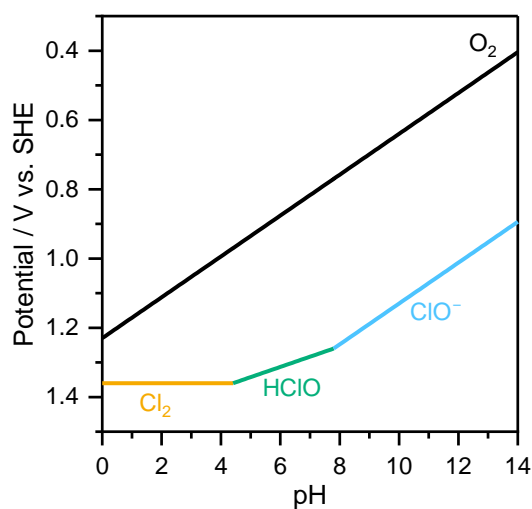
$$2H_2O \rightarrow O_2 + 4(H^+ + e^-). \qquad (S2)$$

Fig. S1 Potential gaps between the evolution reactions of O_2, Cl_2, HClO, and ClO^- as a function of pH.
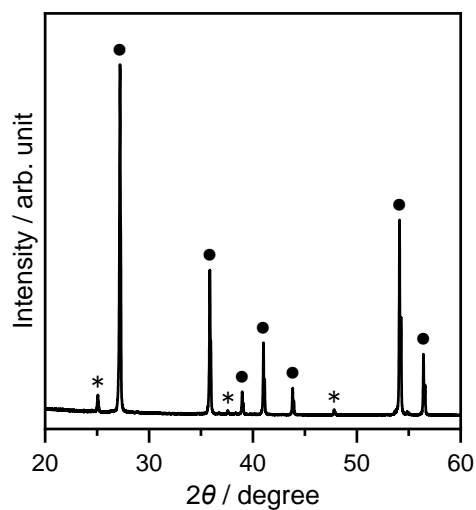
Fig. S2 XRD pattern of TiO_2. Closed circles and asterisks indicate diffraction peaks assigned to the rutile and anatase phases, respectively.
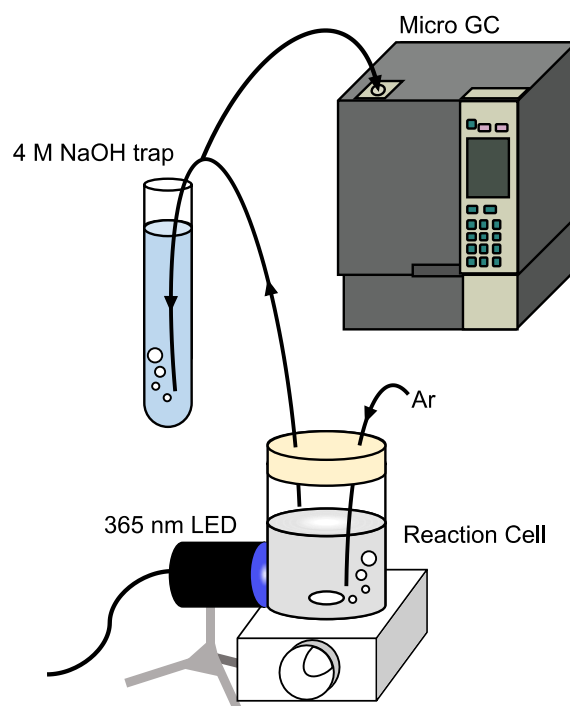

Fig. S3 Schematic of the flow-type photocatalytic reaction system with 5 mL min^{-1} Ar gas flow, showing the evolved Cl_2 gas being trapped in a 4 M NaOH solution.
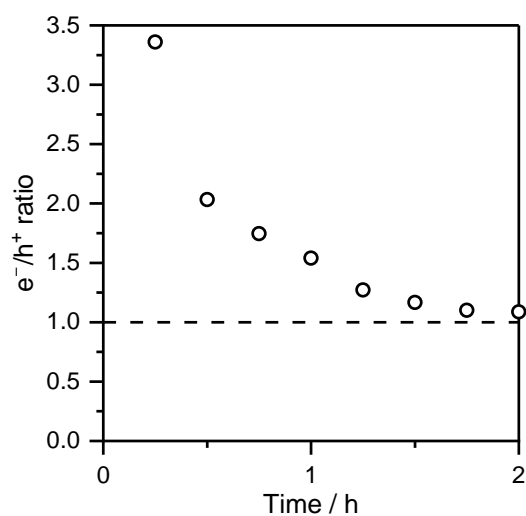
Fig. S4 Time-dependent e^-/h^+ ratio of the products generated in an aqueous NaCl solution at pH 1 (corresponding to Fig. 2(A)). The dashed line indicates the e^-/h^+ ratio for a stoichiometric reaction.

Table S1 Control experiments of TiO_2 photocatalyst for brine splitting.

| Entry | Condition | Amounts of gasses (1 h) / μmol | | | e^-/h^+ |
		H_2	O_2	Cl_2	
1	Standard[a]	12.7	1.4	10.3	0.97
2	Without photocatalyst	0	0	0	–
3	Adjusting the acidity with H_2SO_4	10.5	0.3	9.3	1.1
4	Without Pt-modification	0	0	0	–
5	Using anatase TiO_2 instead of rutile	0	0	0	–

[a] Reaction conditions: catalyst, 10 mg; solution, 500 mM NaCl aq. (30 mL, pH adjusted with $HClO_4$); light source: 365 nm LED.
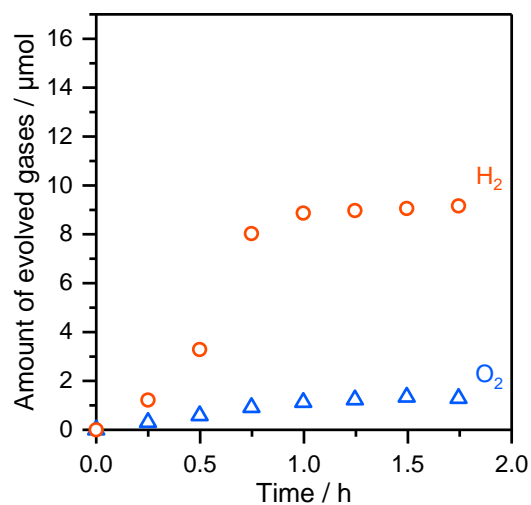
Fig. S5 Time courses of brine splitting with 0.1 wt% Pt-loaded TiO$_2$ in a closed batch-type photocatalytic reaction system. Reaction conditions: catalyst, 100 mg; solution, 500 mM NaCl aq. (300 mL, pH 1); light source: 365 nm LED.
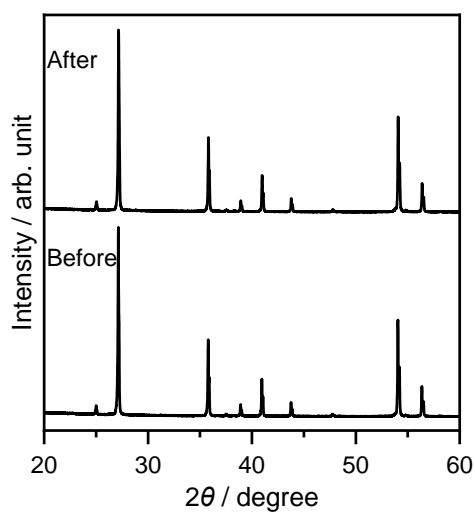

Fig. S6 XRD patterns of Pt-loaded TiO$_2$ before and after the 1h of brine splitting reaction.
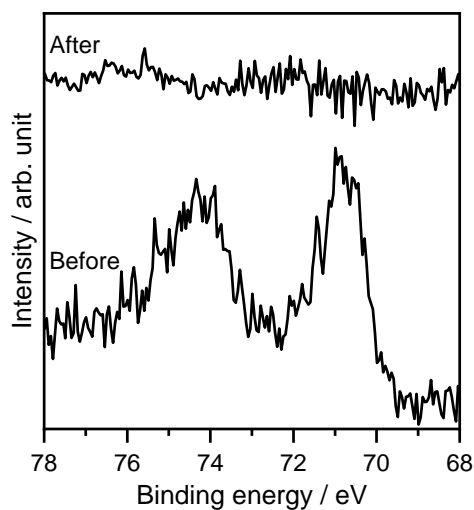
Fig. S7 XPS spectra for Pt4f of Pt-loaded TiO_2 before and after the 1h of brine splitting reaction.
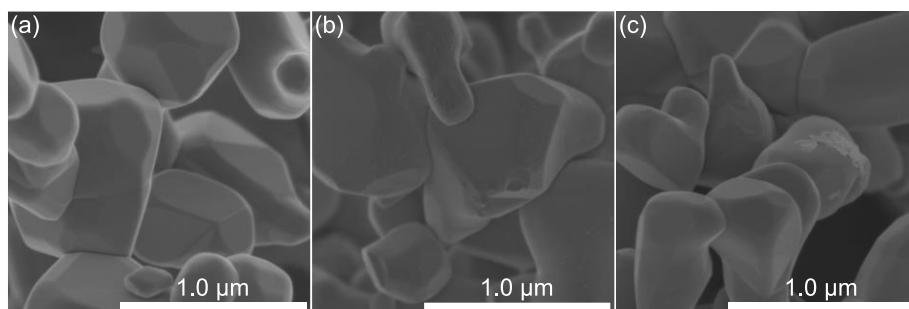

Fig. S8 SEM images of (a) TiO_2, Pt-loaded TiO_2 (b) before and (c) after the 1h of brine splitting reaction.
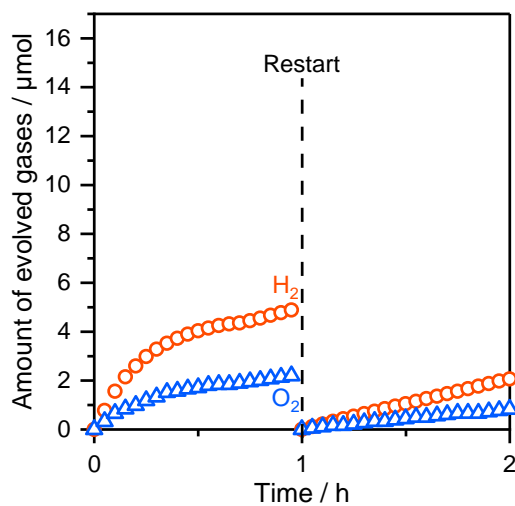

Fig. S9 Time courses of water splitting without NaCl over 0.1 wt% Pt-loaded TiO_2 at pH 1. Reaction conditions: catalyst, 10 mg; solution, H_2O (30 mL, pH1); light source: 365 nm LED.

Table S2 Comparison of the Pt-loaded TiO$_2$ prepared in this study with other brine splitting photocatalyst systems.

| Photocatalyst	Cocatalyst	Solution	Light source	Activity / μmol h^{-1}		Production of Cl$^-$ oxidant	Performance better than in pure water	Ref.
				H$_2$	O$_2$			
TiO$_2$	Pt	3.5% NaCl (pH 1)	365 nm LED	12.7	1.4	Yes	Yes	Present study
P25	CuO	3.5% NaCl	300 W Xe	0.31	–	–	–	14
Brookite TiO$_2$	Pt	Artificial seawater	500 W Hg	0.72	Not detected	No	No	15
La$_2$Ti$_2$O$_7$	NiO/Ni	Seawater	400 W Hg	69.6	34.8	No	No	16
Cd$_4$P$_2$Br$_3$	–	Seawater (1 M NaOH)	400 W Hg ($\lambda > 395$ nm)	0.1	–	No	No	17
(Ga$_{1-x}$Zn$_x$)(N$_{1-x}$O$_x$) ($x = 0.12$)	Rh$_{2-y}$Cr$_y$O$_3$	Artificial seawater	450 W Hg ($\lambda > 400$ nm)	105	30	Yes	No	18
CDots-C$_3$N$_4$	–	Seawater	300 W Hg ($\lambda > 420$ nm)	11.1	5.54	No	No	19
InGaN/GaN	Rh/Cr$_2$O$_3$, Co$_3$O$_4$	3.5% NaCl	300 W Xe (AM 1.5G)	2.4 $\times 10^3$	1.2 $\times 10^3$	No	No	20
p-GaN/InGaN	Rh/Cr$_2$O$_3$,	Artificial seawater	300 W Xe (AM 1.5G)	1.9–2.4 $\times 10^3$	9.5 $\times 10^2$ to 1.2 $\times 10^3$	Yes	Yes	21
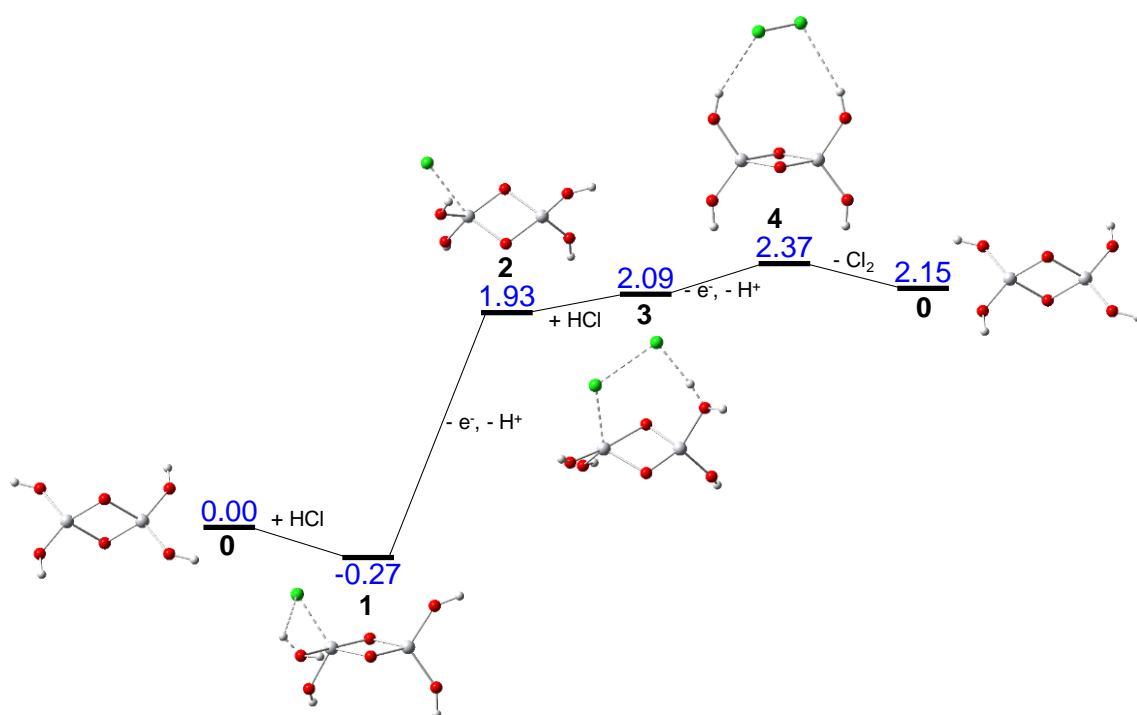
Fig. S10 Intermediate structures and free energies (eV) of HCl oxidation on rutile TiO$_2$. White, red, green, and grey spheres represent H, O, Cl, and Ti, respectively.
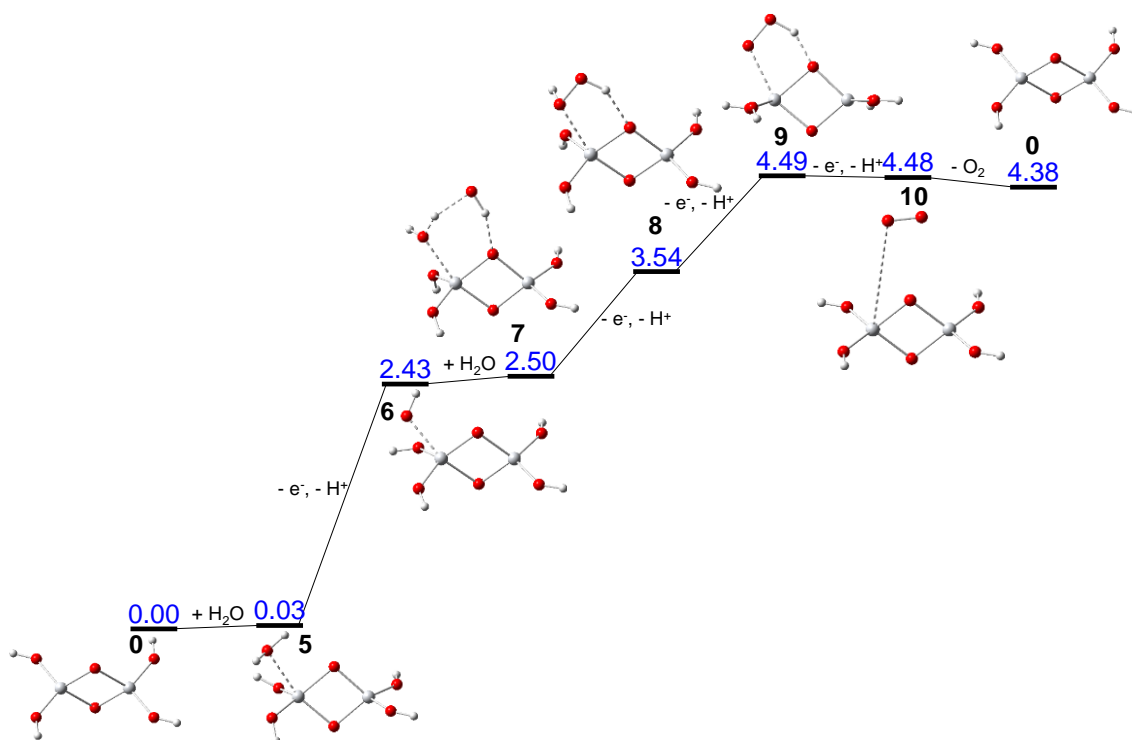
Fig. S11 Intermediate structures and free energies (eV) of H_2O oxidation on rutile TiO_2. White, red, and grey spheres represent H, O, and Ti, respectively.

Table S3 ΔG values for the PCET steps in the mechanism underlying the photoinduced oxidation.

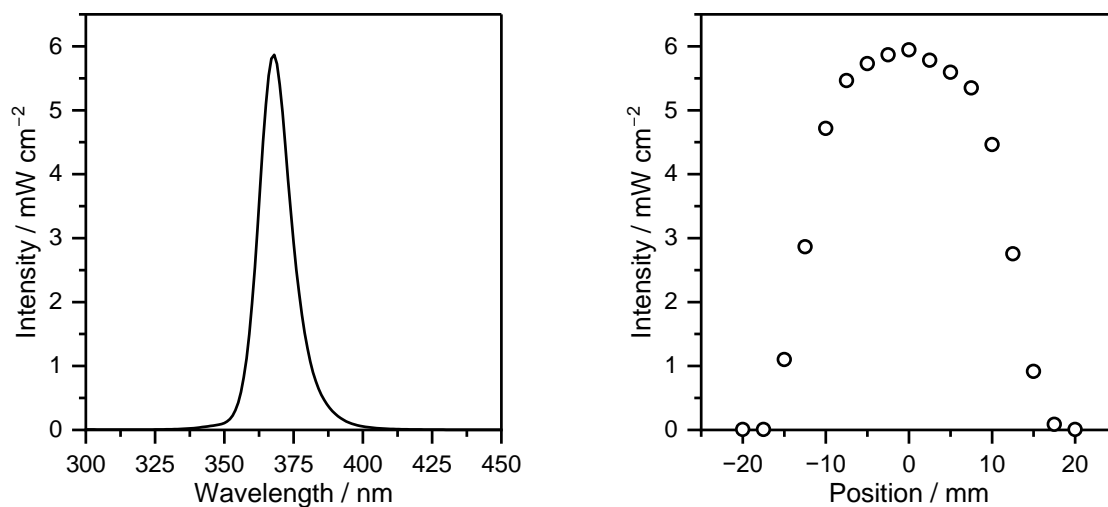| Reactant	Step	ΔG / eV
HCl	**1→2**	2.20
HCl	**3→4**	0.28
H_2O	**5→6**	2.40
H_2O	**7→8**	1.04
H_2O	**8→9**	0.95
H_2O	**9→10**	−0.01

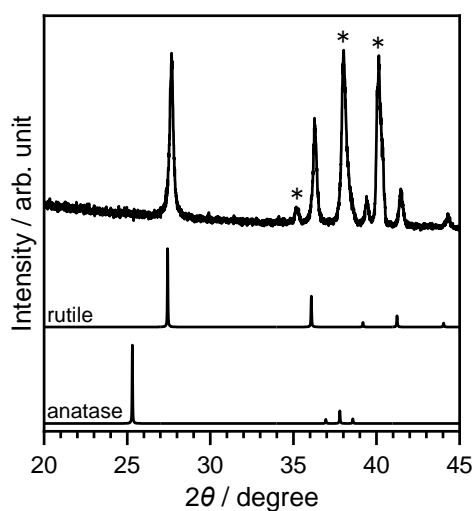**Fig. S12** Power spectrum of the 365 nm LED lamp acquired using a detector-to-lamp distance of 4 cm.

Fig. S13 XRD pattern of electrode obtained by calcining Ti plate at 973 K in air for 1 h. Asterisks indicate diffraction peaks assigned to the Ti substrate.

References

1 M. J. Frisch, G. W. Trucks, H. B. Schlegel, G. E. Scuseria, M. A. Robb, J. R. Cheeseman, G. Scalmani, V. Barone, G. A. Petersson, H. Nakatsuji, X. Li, M. Caricato, A. V. Marenich, J. Bloino, B. G. Janesko, R. Gomperts, B. Mennucci, H. P. Hratchian, J. V. Ortiz, A. F. Izmaylov, J. L. Sonnenberg, D. Williams-Young, F. Ding, F. Lipparini, F. Egidi, J. Goings, B. Peng, A. Petrone, T. Henderson, D. Ranasinghe, V. G. Zakrzewski, J. Gao, N. Rega, G. Zheng, W. Liang, M. Hada, M. Ehara, K. Toyota, R. Fukuda, J. Hasegawa, M. Ishida, T. Nakajima, Y. Honda, O. Kitao, H. Nakai, T. Vreven, K. Throssell, J. A. Montgomery Jr., J. E. Peralta, F. Ogliaro, M. J. Bearpark, J.

J. Heyd, E. N. Brothers, K. N. Kudin, V. N. Staroverov, T. A. Keith, R. Kobayashi, J. Normand, K. Raghavachari, A. P. Rendell, J. C. Burant, S. S. Iyengar, J. Tomasi, M. Cossi, J. M. Millam, M. Klene, C. Adamo, R. Cammi, J. W. Ochterski, R. L. Martin, K. Morokuma, O. Farkas, J. B. Foresman and D. J. Fox, *Gaussian 16, Revision C.02*, Gaussian, Inc., Wallingford CT, 2019.

2   A. D. Becke, *J. Chem. Phys.*, 1993, **98**, 5648–5652.

3   C. Lee, W. Yang and R. G. Parr, *Phys. Rev. B*, 1988, **37**, 785–789.

4   R. Krishnan, J. S. Binkley, R. Seeger and J. A. Pople, *J. Chem. Phys.*, 1980, **72**, 650–654.

5   P. J. Hay, *J. Chem. Phys.*, 1977, **66**, 4377–4384.

6   H. Kusama, M. Kodera, K. Yamashita and K. Sayama, *Phys. Chem. Chem. Phys.*, 2022, **24**, 5894–5902.

7   X. Zhang, Y. Liu, X. Ma, F. Jin, B. Abulimiti and M. Xiang, *Optik*, 2020, **221**, 165395.

8   Y. Miseki and K. Sayama, *Adv. Energy Mater.*, 2019, **9**, 1801294.

9   S. Yanagida, S. Yanagisawa, K. Yamashita, R. Jono and H. Segawa, *Molecules*, 2015, **20**, 9732–9744.

10 Y. Nosaka and A. Nosaka, *ACS Energy Lett.*, 2016, **1**, 356–359.

11 Y. Nosaka and A. Y. Nosaka, *Chem. Rev.*, 2017, **117**, 11302–11336.

12 S. Yanagida, S. Yanagisawa, K. Yamashita, R. Jono and H. Segawa, *ECS Trans.*, 2017, **80**, 1091–1112.

13 Y. Nakabayashi, N. Suzuki, C. Terashima and A. Fujishima, *J. Phys. Chem. C*, 2021, **125**, 18579–18587.

14 A.-J. Simamora, T.-L. Hsiung, F.-C. Chang, T.-C. Yang, C.-Y. Liao and H. P. Wang, *Int. J. Hydrogen Energy*, 2012, **37**, 13855–13858.

15 S. Cao, T.-S. Chan, Y.-R. Lu, X. Shi, B. Fu, Z. Wu, H. Li, K. Liu, S. Alzuabi, P. Cheng, M. Liu, T. Li, X. Chen and L. Piao, *Nano Energy*, 2020, **67**, 104287.

16 S. M. Ji, H. Jun, J. S. Jang, H. C. Son, P. H. Borse and J. S. Lee, *J. Photochem. Photobiol. A*, 2007, **189**, 141–144.

17 M. M. Ayyub, M. Chhetri, U. Gupta, A. Roy and C. N. R. Rao, *Chem. Eur. J.*, 2018, **24**, 18455–18462.

18 K. Maeda, H. Masuda and K. Domen, *Catal. Today*, 2009, **147**, 173–178.

19 J. Liu, Y. Liu, N. Liu, Y. Han, X. Zhang, H. Huang, Y. Lifshitz, S.-T. Lee, J. Zhong and Z. Kang, *Science*, 2015, **347**, 970–974.

20 P. Zhou, I. A. Navid, Y. Ma, Y. Xiao, P. Wang, Z. Ye, B. Zhou, K. Sun and Z. Mi, *Nature*, 2023, **613**, 66–70.

21 X. Guan, F. A. Chowdhury, N. Pant, L. Guo, L. Vayssieres and Z. Mi, *J. Phys. Chem. C*, 2018, **122**, 13797–13802.